Journal of ELECTRONIC MATERIALS, Vol. 48, No. 3, 2019
https://doi.org/10.1007/s11664-018-06916-7

Fascinating Physical Properties of 2D Hybrid Perovskite $[(NH_3)(CH_2)_7(NH_3)]CuCl_xBr_{4-x}$, $x = 0$, 2 and 4

SEHAM K. ABDEL-AAL[1,2,3] and AHMED S. ABDEL-RAHMAN[1,2,4]

1.—Physics Department, Faculty of Science, Cairo University, Giza 12613, Egypt. 2.—Egypt Nano-Technology Center EGNC, Cairo University Campus in Shikh Zayed City, Giza, Egypt. 3.—e-mail: seham@sci.cu.edu.eg. 4.—e-mail: asabry@sci.cu.edu.eg

The 2-D organic–inorganic hybrid perovskites of the formula $[(NH_3)(CH_2)_7(NH_3)]CuCl_xBr_{4-x}$, $x = 0$, 2 and 4 were prepared by slow evaporation from ethanolic solution in stoichiometric ratio 1:1 (organic/inorganic). Microchemical analysis and x-ray diffraction (XRD) were used to confirm the formation of the presently investigated hybrids. Differential scanning calorimetry (DSC) indicated order–disorder transitions at $T_1 = 357$ K, $T_2 = 388$ K, and $T_3 = 398$ K for $x = 0$, 2 and 4 of the three heptain diammonium Cu hybrid perovskites, respectively. These transitions are in good agreement with the electrical permittivity results at different frequencies and temperatures. Optical properties and estimated band gap energy reveal that the band gap energy decreases sharply with replacement of Cl ion by Br ion where the band gap energy of $[(NH_3)(CH_2)_7(NH_3)]CuBr_4$, $x = 0$ (denoted 2C7CuBr) is 1.6 eV (brown color) and for $[(NH_3)(CH_2)_7(NH_3)]CuCl_4$, $x = 4$ (denoted 2C7CuCl) is 2.6 eV (yellow color). The differential magnetic susceptibility of 2C7CuBr in the temperature range 80–300 K indicates the effective magnetic moment $\mu_{eff} = 2.05$ BM.

Key words: 2D hybrid perovskite, optical properties of halide perovskite, phase transition, magnetic properties of Cu perovskite

INTRODUCTION

The 2-D hybrid perovskites of the formula A_2MX_4, *A*: ammonium substituted organic cation, *M*: a divalent metal ion and *X*: a halogen (Cl, Br, I)[1–19] have drawn considerable attention recently. Its applications include smart microelectronic, optoelectronic, exitonic and self assembly quantum wells.[14,20–22] The properties of these hybrid perovskites (OIHs) are functions of *A*, *M* and *X* and there are possibilities to tailor its structure, physical and chemical properties according to the technological application needed.[15,19,20,22,23] The 2-D hybrid nanocomposites of the formula $[(NH_3)(CH_2)_n(NH_3)]MX_4$ denoted $2C_nMX_4$, where, $n = 2$, 3, 4, …, *M* = Mn,[1,2] Co,[5,9,11,16,19] Cd,[6,12] Cu,[4,8,15,24–28] Pb,[7,14] pd[8] and Sn[10] are referred to diammonium hybrid perovskites, where the two NH_3 groups attached to both ends of the organic moiety. The monoammonium hybrid perovskites (bilayers) with formula $[C_nH_{2n+1}(NH_3)]_2MX_4$ for short C_nMX_4, *M* = Ge, Pb, Sn,[20] Cu,[21,29,30] are where each of both organic moieties are attached at one end to the NH_3 group. The 2-D hybrid perovskites are characterized by an alternating structure where the metal halide layers are sandwiched between alkylammonium chains. The crystal structure of these hybrid perovskites is stabilized by a series of hydrogen bonds and van der Waals interactions between anions and cations. The ammonium ion at the end of organic chains forms N–H…*X* hydrogen bonds with the halide ion of the metallic layer. The 2-D hybrid perovskites of diammonium series could be used in photovoltaic applications, ultraviolet (UV) detection and catalytic activity.[15,30–32] These materials tend to exhibit a number

(Received June 25, 2018; accepted December 29, 2018; published online January 9, 2019)

of phase transitions such as solid–solid phase transitions and order–disorder transitions.[16,17,33]

Previous studies of the structure, electrical and magnetic properties of some members of the ammonium perovskite hybrids of both mono and diammonium series where M = Cu showed interesting results.[4,8,15,21,24–29]

No results are observed for moderate chain length $n = 7, M$ = Cu for the diammonium series of 2-D hybrid perovskites. The objectives of this work are synthesis, characterization and studying of some physical properties including thermal, electrical, optical and magnetic of the newly prepared hybrid perovskites $[(NH_3)(CH_2)_7(NH_3)]CuCl_xBr_{4-x}$, $x = 0$, 2 and 4.

EXPERIMENTAL PROCEDURES

Preparation of the Materials

All chemicals were purchased from SIGMA-ALDRICH and used as received. The purity of the used products is exceeding 99%. Solvents were of the reagent grade.

The synthesis of diammonium $[(NH_3)$-R-$(NH_3)]MX_4$, and monoammonium perovskite hybrids $[R\text{-}(NH_3)]_2MX_4$ where R; organic group, M, X, proceed as described in Refs. 15–19 in two stages according to the following equations

$$\begin{matrix}[(NH_2)-R-(NH_2)] & & [(NH_3)-R-(NH_3)]Cl_2 \\ & +2HCl \xrightarrow{\Delta} & \\ 2[R-(NH_2)] & & 2[R-(NH_3)]Cl\end{matrix} \quad (1)$$

$$\begin{matrix}[(NH_3)-R-(NH_3)]Cl_2 & & [(NH_3)-R-(NH_3)]MCl_4 \\ & +MCl_2 \xrightarrow{\Delta} & \\ 2[R-(NH_3)]Cl & & [R-(NH_3)]_2MCl_4\end{matrix} \quad (2)$$

The prepared materials recrystallized twice for further purification then were dried under vacuum. Chemical analysis for C, H, Cu% was carried out and tabulated in Table I, it shows that the newly prepared hybrids have the correct chemical formula $[(CH_2)_7(NH_3)_2]CuCl_xBr_{4-x}$, $x = 0$, 2 and 4 where here they will be donated 2C7CuCl, 2C7CuCB and 2C7CuBr, respectively.

Characterization

X-ray Powder Diffraction Measurement

The x-ray diffraction (XRD) powder data were collected using a computer controlled Siemens (D5000) powder x-ray diffractometer with CuKα radiation λ = 1.54056 Å. The measuring range (2θ) from 5° to 55° and the instrumental resolution was 0.004–0.005° at room temperature. Data collections were performed in step-scan mode with steps of 0.02°.

Thermal Analysis (Differential Scanning Calorimetry DSC)

Thermal characteristics of 2C7CuCl, 2C7CuCB and 2C7CuBr in the temperature range 300–420 K were performed using a differential thermal scanner Shimadzu-60 at a scanning speed of 5°C/min. The analyzer was calibrated with the melting transition of indium at 157°C. Measurements were performed in a flow of dry nitrogen gas and data were collected during the heating run.

Physical Properties

Electrical Properties (Permittivity Measurements)

The complex dielectric permittivity ε^* in the frequency range 2.01–200 kHz in temperature range 300–420 K were measured using a computer controlled LCR HITESTER 3532-50 HIOKI. The temperature was measured using a copper constantan thermocouple. The samples are in the form of compressed pellets of 10 mm in diameter and 1.2 mm thick. The pellets surfaces were coated with a thin layer of silver paste to ensure good electrical contact. All measurements were carried out while heating up the sample with rate 0.5°C/min in an evacuated homemade silica glass cryostat.

Optical Properties

The UV–Vis absorption and diffuse reflectance spectrum were recorded at room temperature. The data were collected using UV–visible (Vis)–near infrared (NIR) spectro-photometer type Jasco-V-570 spectrophotometer, Japan, fitted with an integrating sphere reflectance unit (ISN) in the wavelength range 200–2000 nm.

Table I. The chemical analysis of $[(CH_2)_7(NH_3)_2]CuCl_xBr_{4-x}$, $x = 0$, 2 and 4

	C%			H%			Cu%		
Materials	**Calc**	**Found**	**Error**	**Calc**	**Found**	**Error**	**Calc**	**Found**	**Error**
2C7CuCl	24.88	24.56	1.28	5.92	5.25	11.31	18.81	18.52	1.54
2C7CuCB	19.69	20.11	2.13	4.69	4.97	5.97	14.90	15.20	2.01
2C7CuBr	16.29	16.01	1.71	3.88	4.10	5.67	12.32	11.97	2.84

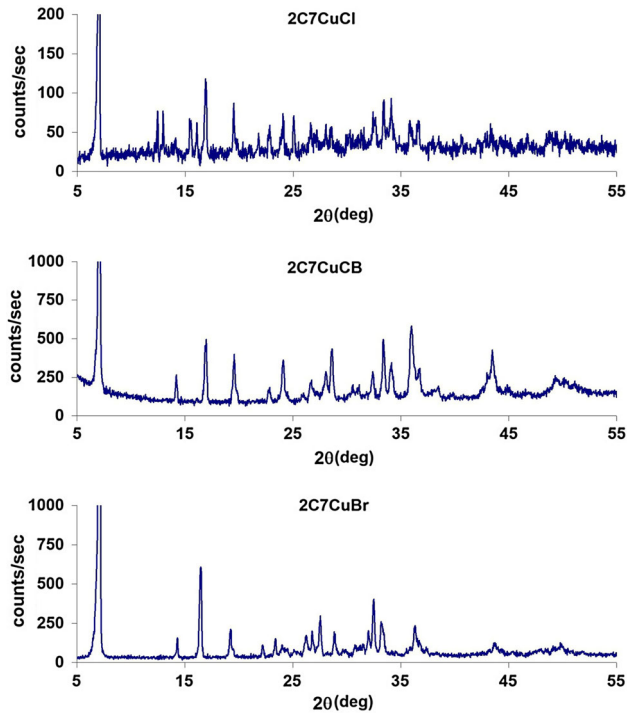

Fig. 1. XRD of 2C7CuCl, 2C7CuCB and 2C7CuBr.

Magnetic Susceptibility Measurements

The differential magnetic susceptibility was measured in the temperature range 80–300 K at frequency of 320 Hz in a magnetic field of 5 Oe using a Lakeshore 7000-series AC Susceptometer/Magnetometer. The basic principle for measuring the ac susceptibility is that the self-inductance of a coil or the mutual inductance of a set of two coils changes if one inserts a magnetic material in the core of the coil.

RESULTS AND DISCUSSION

X-ray Diffraction and Crystal Structure

The XRD diffraction patterns of 2C7CuCl, C7CuCB and 2C7CuBr are shown in Fig. 1. The structure and crystallographic information of currently investigated hybrids were discussed in our previous work.[15] The structure of other members of diammonium series of shorter organic chain lengths $[(CH_2)_n(NH_3)_2CuX_4]$ x = Cl, Br; n = 2, 3, 4, 5 are reported in Refs. 4, 24 and 25. Briefly, the structure of a Cu hybrid consists of corner shared octahedral distorted $[CuX_6]^{-2}$, x = Cl, Br anion and $[(NH_3)(CH_2)_7(NH_3)]^{+2}$ cations. It consists of the aliphatic chain extended in a zigzag structure of carbon atoms with two NH_3 cations that are

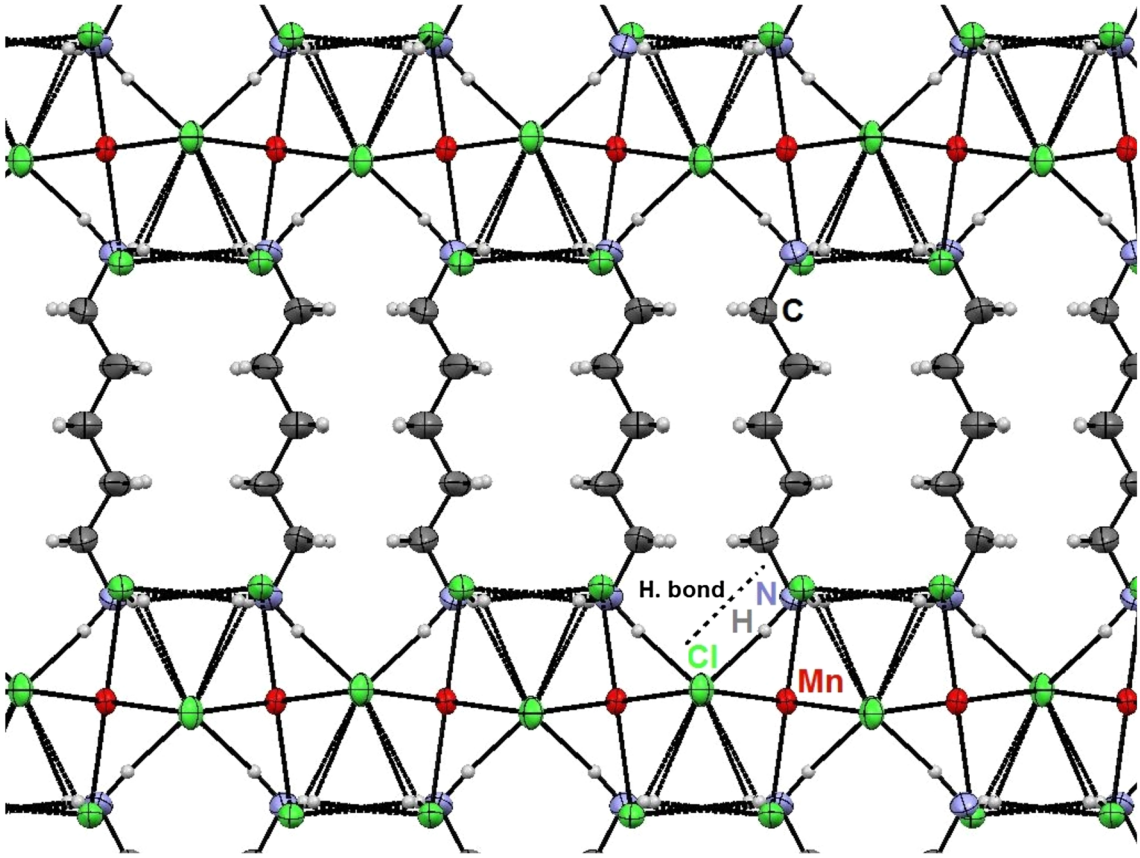

Fig. 2. Layered structure and H. bond of $(NH_3(CH_2)_5NH_3)MnCl_4$ along *a* axis.

attached to both chain ends. The hydrogens of NH_3 group are bonded to the halide anion. We tried to grow single crystals of the presently investigated hybrids; we did not obtain suitable crystals for a single crystal diffractometer. Figure 2[34] shows the crystal structure of $[(CH_2)_5(NH_3)_2MnCl_4]$ from single crystal x-rays which are isomorphs to the current Cu-hybrid, from our previous work[32] for clarification. The halide substitution has observable effect on the structure of $[(NH_3)(CH_2)_7(NH_3)]CuCl_xBr_{4-x}$, $x = 0$, 2 and 4. The replacement of Cl by Br increases the H. bond length as observed before in shorter organic chain lengths.[4,15] It also affects the unit cell volume and octahydron bond length.[4] This will affect the physical properties as will be seen in sections below. The average crystallite size was determined using the Debye–Scherrer's equation[35] and shown in Table II.

Differential Scanning Calorimetry (DSC)

The DSC thermographs of 2C7CuCl, 2C7CuCB and 2C7CuBr hybrids are shown in Fig. 3. The three main transitions indicated by arrows are endothermic peaks at $T_1 = 398 \pm 2$ K, $T_2 = 388 \pm 2$ K and $T_3 = 357 \pm 1$ K for 2C7CuCl, 2C7CuCB and 2C7CuBr, respectively. These transitions possess high entropy values which are usually associated with order–disorder phase transitions. The temperatures and entropies of these transitions are listed in Table III as well as members of previously investigated diammonium Cu hybrid perovskite of shorter and longer organic chain lengths for comparison. The transitions at below 340 K are attributed to reorientation of organic chains usually this transition is called "chain melting"[36] where one or more bonds gauche up and down the organic chain.[37] The transitions above 360 K belong to the inorganic part $[CuX_4]^{-2}$ octahydron. It is clearly seen from Table III, that, as the organic chain length increases, the transition temperature shifts to lower values and also when introducing Br ion replacing Cl. This can be attributed to the structure of the Cu hybrid perovskite changing at different organic chain lengths. As the organic diammonium chain length increases the H. bond length increases also as reported before in our previous work.[15] As the H. bond length increases, the bond strength decreases, so less amount of thermal energy is needed for the hybrid of longer organic chain length to perform phase transition. For the shaded rows of Table III, the substitution of Br ion instead of Cl ion, the transition temperature decreases and this can be explained by the nature of H. bonds strengths for N–H…Br which is weaker than N–H…Cl.

DSC and x-ray results of previously investigated hybrid perovskites indicate that the first order nature of chain melting transitions and the temperature of the chain melting transition depends on the organic chain not on the metal halide.[16,27,36,37]

Table II. Average crystallite size (nm) of $[(NH_3)(CH_2)_7(NH_3)]CuCl_xBr_{4-x}$, $x = 0$, 2 and 4

	Average crystallite size (nm)
2C7CuCl	31
2C7CuCB	35
2C7CuBr	41

Permittivity Results

The temperature dependence of real part of the complex dielectric permittivity (ε') in the temperature range 298–410 K in the frequency range 2.01–200 kHz for the three investigated Cu hybrids are shown in Fig. 4. It is noted that, the value of ε' decreases with the increases of the frequency as in

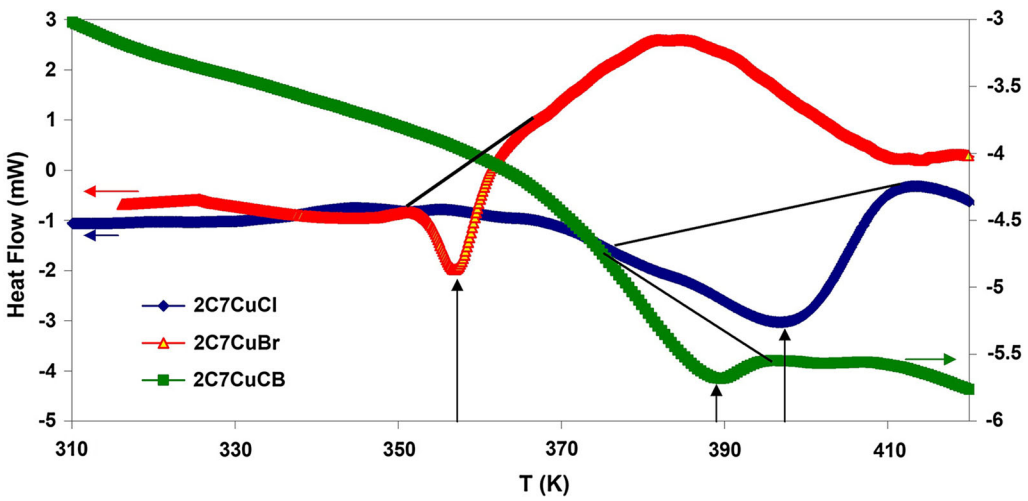

Fig. 3. Differential scanning calorimetry of 2C7CuCl, 2C7CuCB and 2C7CuBr at the temperature range 310–420 K.

Table III. Transition temperatures (K) and entropies ΔS (J/K mol) of hybrids $[(NH_3)\text{-}(CH_2)_n\text{-}(NH_3)]CuCl_4$ denoted $2C_nCuCln$ = 3, 4, 7, 9 and 12

	Transition 1		Transition 2		
Hybrid	***T* (K)**	**ΔS (J/K mol)**	***T*(K)**	**ΔS (J/K mol)**	**References**
2C3CuCl	434	1.53	333.5	3.82	Ref. 28
2C4CuCl	423	…	328	3.25	Ref. 36
2C7CuCl	398	18.07	330	4.94	This work
2C7CuCB	388	7.55	#	#	This work
2C7CuBr	357	6.71	#	#	This work
2C9CuCl	383	3.80	303	…	Ref. 27
2C12CuCl	359	5.8	…	…	Ref. 26

… Not reported in the reference. # Not observed in the measurement.

polar materials, i.e., ε' is a function of temperature and frequency. Starting from the lower temperature side, ε' starts to rise gradually with temperature showing a broad hump at T = 330 K clearly seen at lower frequency and attributed to organic chain melting mentioned above. The ε' starts to increase gradually with a high rate as temperature increases forming a sharp peak centered at T = 397 K with ε' value of 3300 at f = 2.01 kHz for 2C7CuCl. Similar behaviors are obtained for the 2C7CuCB and 2C7CuBr but the transition temperatures are 367 K and 356 K, respectively. The increase of ε' below transition temperature is due to an increase of the polarization arising from the facilitation of the molecular motion within the hybrid, leading to easy orientation of the dipolar units. As the temperature rises further; ε' starts to fall indicating lack of the dipolar interaction. The observed anomalous changes of ε' are in a good agreement with DSC-transition temperatures discussed above. Similar behaviors of permittivity results were obtained from our previous work for Co hybrid perovskite of the same organic chain length.[16–18,33]

Optical Properties

The diffuse reflectance spectrum (DRS) is a spectroscopic technique based on the reflection of light in NIR, Vis and UV regions by a powdered sample. In a DRS the ratio of the light scattered from a thick sheet of the sample and that from an ideal nonabsorbing reference sample is measured as a function of the wavelength λ (i.e., F_{SKM} (R_∞) versus λ nm). Whereas the relation between the diffuse reflectance of the sample (R_∞), absorption (K) and scattering (S) coefficients are correlated by the Schuster–Kubelka–Munk (SKM) remission function

$$F_{SKM}(R_\infty) = (1-R_\infty)^2/2R_\infty = K/S. \qquad (3)$$

The band gap E_g is determined from the optical reflectance spectra by extrapolating the straight line plot of $(F(R_\infty)\cdot h\upsilon)^n$ versus $(h\upsilon)$ according to the following Kubelka–Munk equation

$$(F(R_\infty)\cdot h\upsilon)^n = A\left(h\upsilon - E_g\right), \qquad (4)$$

where h is the Plank's constant, υ is the frequency of the vibration and A is a constant. The exponent n depends on the type of the transition and takes the value 1/2 or 3/2 for the indirect transitions, while 2 or 3 for the direct allowed transitions.[38–40]

Figure 5 shows the optical properties of 2C7CuBr. The sample shows a strong absorption at the UV–Vis light region, so this behavior may find attractive applications as visible light photocatalysis. The spectra exhibits two distinct absorptions bands centered at 464 nm and 820 nm. Table IV shows the band gap energy of 2C7CuCl, 2C7CuCB and C7CuBr. One can see that, the band gap energy decreases with increasing the Br content at the same organic chain length and this can be attributed to the difference in energy levels in the three Cu hybrids. The H. bond lengths which links $[CuCl_4]^{6-}$, $[CuCl_2Br_2]^{6-}$, $[CuBr_4]^{6-}$ octahedron with the organic diammonium part are different where the longer and the weaker H. bond length were reported to the $[(NH_3)(CH_2)_5(NH_3)]CuBr_4$ hybrid.[4,15] It is worth to mention that the H. bond and the octahydron $[CuX_4]^{6-}$ x = Cl, Br are responsible for the charge transport inside the investigated hybrids. The band gap energy of 2C7CuBr is very promising for the photovoltaic applications.[30]

Magnetic Properties

The magnetic properties were measured for the substituted Br^- ion (x = 0) of the heptane diammonium Cu hybrid 2C7CuBr. The Br^- substantial has ionic radius nearly doubled than that of Cl^- which leads to a larger overlap of electron density and thus

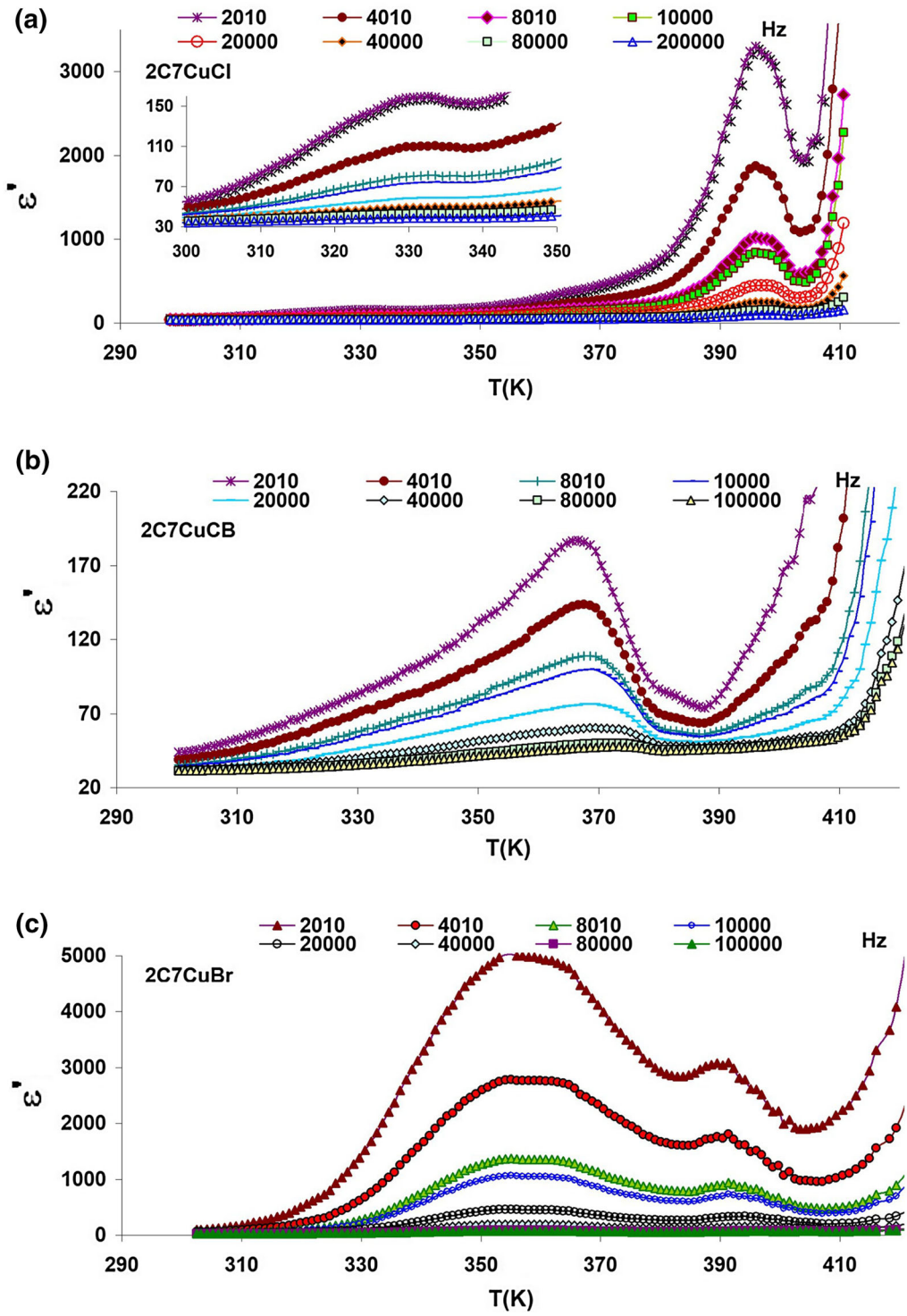

Fig. 4. Temperature dependence of the real part of the electrical permittivity ε' in the temperature range 300–420 K in the frequency range 2.01–200 kHz of (a) 2C7CuCl, (b) 2C7CuCB, (c) 2C7CuBr.

leading to a stronger magnetic coupling.[25] Figure 6 shows the variation of the molar magnetic ac susceptibility χ_M and its reciprocal $1/\chi_M$ as a function of temperature (70–310 K) in an ac field of 5 Oe and frequency $f = 320$ Hz. The magnetic susceptibility increases gradually as the temperature decreases following Curie–Weiss law. The reciprocal susceptibility yields an effective magnetic moment $\mu_{eff} = 2.05$ BM which is in good agreement for Cu^{2+} in an octahedral structure as reported

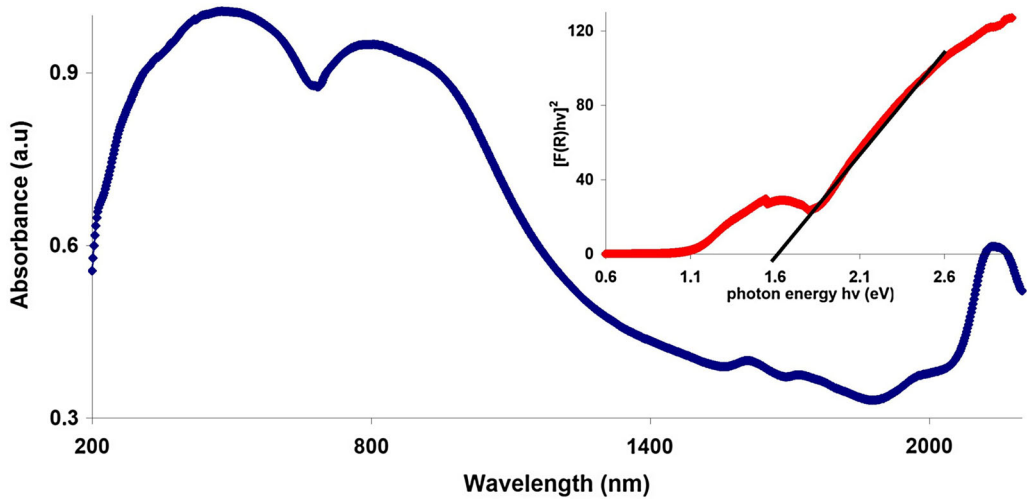

Fig. 5. Optical properties of $[(NH_3)(CH_2)_7(NH_3)]CuBr_4$ spectra absorbance and inset figure is the optical band gap energy.

Table IV. Bandgap energy (eV) of 2C7CuCl, 2C7CuCB and 2C7CuBr

Cu hybrid	2C7CuCl	2C7CuCB	2C7CuBr
Energy gap (eV)	2.6	2.18	1.6
References	Ref. 15	Ref. 15	This work

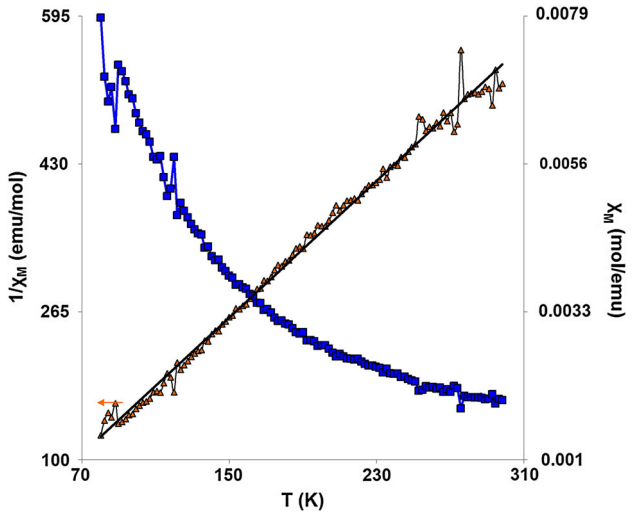

Fig. 6. Corrected molar magnetic susceptibility χ_M and its reciprocal $1/\chi_M$ as a function of temperature 70–310 K of $[(NH_3)(CH_2)_7(NH_3)]CuBr_4$.

Table V. Comparison of the physical properties of the three halide substituted Cu perovskites

Cu hybrid	2C7CuCl	2C7CuCB	2C7CuBr
Crystallite size (nm)	30.61	35.34	41.21
DSC T peak transition (K)	398	388	357
ε' T peak transition (K)	397	367	356
Energy gap (eV)	2.6	2.18	1.6
Color	Yellow	Light brown	Dark brown

before.[21,25,27] Table V shows a comparison of the physical properties of the halide substituted Cu perovskite.

CONCLUSION

The organic–inorganic hybrids of $[(NH_3)(CH_2)_7(NH_3)]CuCl_xBr_{4-x}$, $x = 0$, 2, 4 have been successfully prepared. The 2-D Layered structure consists of a corner shared octahedral of $[CuX4]^{-6}$ x = Cl, Br anions and $[(NH_3)(CH_2)_n(NH_3)]^{+2}$ cations that are connected via H. bonds. Phase transitions were confirmed by DSC and electrical permittivity results indicating order–disorder transition for the three Cu hybrids. A strong absorption in the UV–Vis range and the band gap energy is 1.6 eV for 2C7CuBr, this may find applications in visible light photocatalysis and photovoltaic applications. The effective magnetic moment of $[(NH_3)(CH_2)_7(NH_3)]CuBr_4$ is $\mu_{eff} = 2.05$ BM, which in a good agreement for Cu^{2+} in an octahedral structure.

ACKNOWLEDGMENTS

The authors are grateful to the financial Support of Cairo University, Electromagnetic Lab. Members (Mohga F., Shimaa S., Ahmed K.), and Polymer Technology Lab. Members (Amin S., Hamdy O.). This work has been done at the Physics Department, Faculty of Science, Cairo University. Optical properties were measured at Central Metallurgical Research and Development Institute, Tibeen, Egypt.

REFERENCES

1. K. Tichý, J. Benes, W. Hälg, and H. Arend, *Acta Cryst.* B34, 2970 (1978).
2. K. Tichý, J. Benes, R. Kind, and H. Arend, *Acta Cryst.* B36, 1355 (1980).
3. A. Kallel, J. Fail, H. Fuess, and A. Daoud, *Acta Cryst.* B36, 2788 (1980).
4. J.K. Garland, K. Emerson, and M.R. Pressprich, *Acta Cryst.* C46, 1603 (1990).
5. N. Guo, Y.-H. Lin, G.-F. Zeng, and S.-Q. Xi, *Acta Cryst.* C48, 542 (1992).
6. M. Khechoubi, A. Bendani, N.B. Chanh, C. Courseille, R. Duplessix, and M. Couzi, *J. Phys. Chem. Solids* 55, 1277 (1994).
7. C. Courseille, N.B. Chanh, Th Maris, A. Daoud, Y. Abid, and M. Laguerre, *Phys. Stat. Sol.* A143, 203 (1994).
8. T. Maris, G. Bravic, N.B. Chanh, J.M. Leger, J.C. Bissey, A. Villesuzanne, R. Zouari, and A. Daoud, *J. Phys. Chem. Solids* 57, 1963 (1996).
9. J.J. Criado, A. Jiménez-Sánchez, F.H. Cano, R. Sáez-Puche, and E. Rodríguez-Fernández, *Acta Cryst.* B55, 947 (1999).
10. J. Guan, Z. Tang, and A.M. Guloy, *Chem. Commun.* 18, 1833 (1999).
11. A.H. Mahmoudkhani and V. Langer, *Acta Cryst.* E58, m592 (2002).
12. M.F. Mostafa and A. Hassen, *Phase Trans.* 79, 305 (2006).
13. A. Lamhamdi, E. Mejdoubi, K. Fejfarová, M. Dusek, and B. El Bali, *Acta Cryst.* E65, m215 (2009).
14. K. Pradeesh, G.S. Yadav, M. Singh, and G. Vijaya Prakash, *Mat. Chem. Phys.* 124, 44 (2010).
15. S.K. Abdel-Aal, G. Kocher-Oberlehner, A. Ionov, and R.N. Mozhchil, *Appl. Phys. A* 123, 531 (2017).
16. M.F. Mostafa, S.K. Abdel-Aal, and A.K. Tammam, *Ind. J. Phys.* 88, 49 (2014).
17. S.K. Abdel-Aal, *Solid State Ionics* 303, 29 (2017).
18. M.F. Mostafa, S.S. El-khiyami, and S.K. Abdel-Aal, *J. Mol. Struct.* 1127, 59 (2017).
19. S.K. Abdel-Aal and A.S. Abdel-Rahman, *J. Cryst. Growth* 457, 282 (2017).
20. S. González-Carrero, R.E. Galian, and J. Pérez-Prieto, *Part. Syst. Charact.* 32, 709 (2015).
21. B. Kundys, A. Lappas, M. Viret, V. Kapustianyk, V. Rudyk, S. Semak, Ch Simon, and I. Bakaimi, *Phys. Rev. B* 81, 224434 (2010).
22. D.B. Mitzi, K. Chondroudis, and C.R. Kagan, *IBM J. Res. Dev.* 45, 29 (2001).
23. Z. Cheng and J. Lin, *Cryst. Eng. Commun.* 12, 2646 (2010).
24. D.W. Phelps, D.B. Losee, W.E. Hatfield, and D.J. Hodgson, *Inorg. Chem.* 15, 3147 (1976).
25. K. Halvorson and R.D. Willett, *Acta Cryst.* C44, 2071 (1988).
26. M.F. Mostafa and S.A. El-Hakim, *Phase Trans.* 76, 587 (2003).
27. M.F. Mostafa and A.A.A. Youssef, *Z. Naturforsch.* A59, 35 (2004).
28. M.F. Mostafa, A.A.A. Youssef, S.S. Montasser, and S.S. Khyami, *Z. Naturforsch.* A60, 837 (2005).
29. X. Pan, G. Wu, M. Wang, and H. Chen, *J. Zhejiang Univ. Sci. A* 10, 710 (2009).
30. S.K. Abdel-Aal, A.S. Abdel-Rahman, G. Kocher-Oberlehner, A. Ionov, and R.N. Mozhchil, *Acta Cryst.* A73, c1116 (2017).
31. K. Elmebrouki, S. Tamsamani, J. Aazza, M. Khechoubi, and A. Khmou, *J. Asian Sci. Res.* 1, 216 (2011).
32. P. Mondal, S.K. Abdel-Aal, D. Das, and S.M. Islam, *Catal. Lett.* 147, 2332 (2017).
33. M.F. Mostafa, S.S. ElKhiyami, and S.A. Alal, *Mat. Chem. Phys.* 199, 454 (2017).
34. S.K. Abdel-Aal and A.S. Abdel-Rahman, *The Cambridge Crystallographic Data Centre*, CCDC 1401387 (2015).
35. B.D. Cullity and S.R. Stock, *Elements of X-ray Diffraction*, 3rd ed. (New York: Prentice-Hall, 2001), p. 167.
36. T. Maris, N.B. Chanh, J.-C. Bissey, N. Filloleau, S. Flandrois, R. Zouari, and A. Daoud, *Phase Trans.* 66, 81 (1998).
37. R. Kind, S. Plesko, P. Gunter, J. Roos, and J. Fousek, *Phys. Rev. B* 23, 5301 (1981).
38. A.A. Radhakrishnan and B.B. Beena, *Ind. J. Adv. Chem. Sci.* 2, 158 (2014).
39. J. Essic and R. Mather, *Am. J. Phys.* 61, 646 (1993).
40. R. Williardson and A. Beer, *Optical Properties of III–V Compounds* (New York: Academic, 1967), p. 318.